MEASUREMENT OF CORONAL MAGNETIC TWISTS DURING LOOP EMERGENCE OF NOAA 8069

F. PORTIER-FOZZANI[1], M. ASCHWANDEN[2], P. DÉMOULIN[3], W. NEUPERT[4] and the EIT Team with J.-P. DELABOUDINIÈRE P.I.
[1]*Max Planck Institut fur Aeronomie (MPAE), Max-Planck-Straβe 2, D-37191 Katlenburg-Lindau, Germany*
[2]*Lockheed Martin Palo Alto Advanced Technology Center, Palo Alto, California, U.S.A.*
[3]*DASOP, Observatoire de Paris-Meudon, France*
[4]*NOAA – SEC, Boulder, Colorado, U.S.A.*

(Received 22 May 2001; accepted 4 July 2001)

Abstract. Emerging coronal loops were studied with extreme ultraviolet observations performed by SOHO/EIT on 5 and 6 August 1997 for NOAA 8069. Physical parameters (size and twist) were determined by a new stereoscopic method. The flux tubes were measured twisted when first observed by EIT. After emerging, they de-twisted as they expanded, which corresponds to a minimization of the energy. Different scenarios which take into account the conservation of the magnetic helicity are discussed in relation with structure and temperature variations.

1. Introduction

The solar magnetic field (Solanki, 1998), which drives solar activity, emerges over the photosphere as flux tubes which confine the plasma (Klimchuk and Porter, 1996; Parker, 1974).

Different types of loops with fast or slow evolution – between days up to months – coexist (Bray *et al.*, 1991). Their morphologies can change a lot due to shearing and twisting of the flux tubes. Shear, measured along the inversion line of the vertical field component (between the two footpoints of a bipolar AR), plays a major role in flares as reviewed by Heyvaerts and Hagyard (1991). In other cases, loops are sometimes seen to be twisted which indicates a perturbation from a lower energy state. Energy release within very hot loops observed in X-rays and also highly twisted – i.e., with an S shape called a sigmoid – happens sometimes as flares (Rust and Kumar, 1996). Difficulties in measuring the loop twist accounts for the small number of articles concerning it. With new stereoscopy techniques and the actual resolution of EUV instruments it has become possible to estimate the magnetic helicity by twist measurement.

After describing the instruments and the active region loops (hereafter denoted ARL) that we observed, we explain the stereoscopic method that we used to deduce the 3D shape of the observed EIT loops. We focus this study on the measurement of twist and its evolution with time during the short period of time when the loops

Solar Physics **203:** 289–308, 2001.

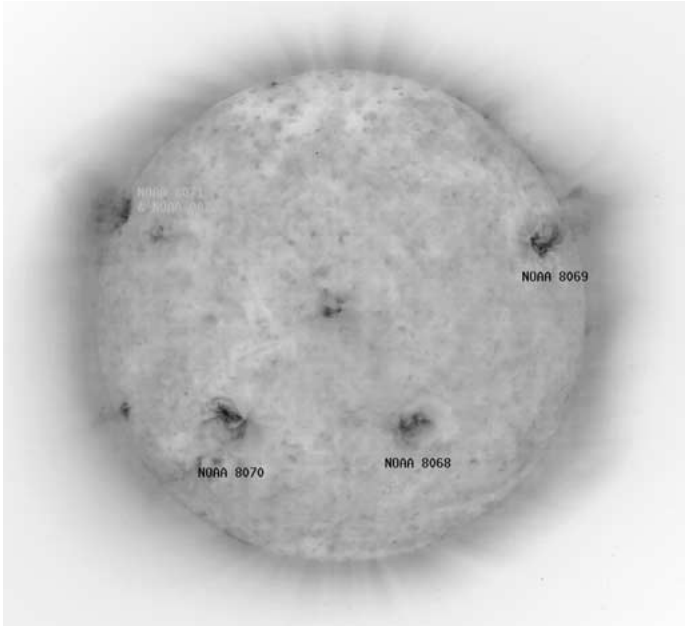

Figure 1. Active regions observed with SOHO/EIT Fe IX/X on 7 August 1997 at 19:54 UT with their NOAA numbers (with reversed intensity table: dark on the figure is bright on the Sun).

emerge. We will then discuss the energy and helicity transfer during the evolution of the geometrical morphology of the loops.

2. Instruments and Target

2.1. Instruments

Multiwavelength observations were used for this study.

– SOHO/EIT images the solar corona in four EUV wavelengths (Delaboudinière *et al.*, 1995). Loops with temperature around 1 MK are clearly visible and their evolution can be studied (e.g., Portier-Fozzani *et al.*, 1997).

– *Yohkoh* SXT images the hot corona in X rays (temperature between 2–10 MK e.g., Uchida, 1992; Bentley, Mariska, and Sakao, 1996).

– Magnetograms: SOHO/MDI gives the longitudinal component of the photospheric magnetic fields with two arc sec resolution for full disk images.

Temperature maps are derived with SOHO/EIT using the atomic CHIANTI code (Dere *et al.*, 1997) with quasi simultaneous image ratios of different EIT filters (Figure 6, cf., Newmark, 1997; Neupert *et al.*, 1998).

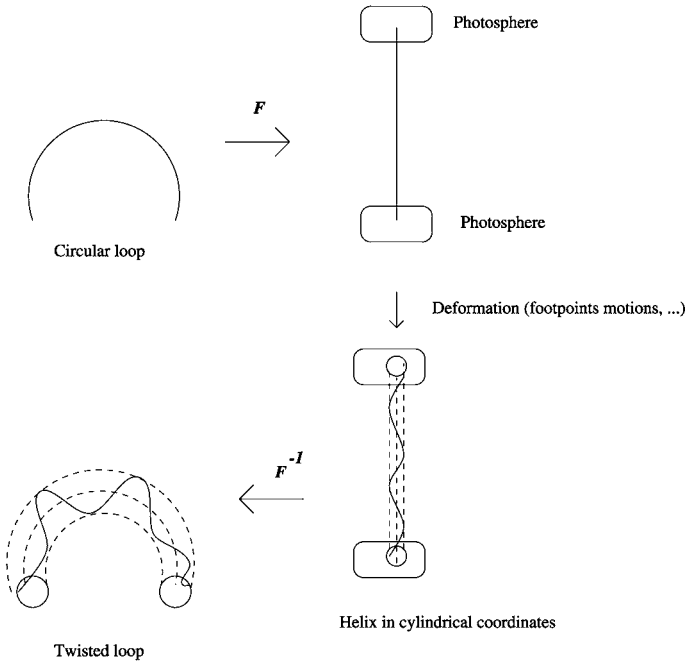

Figure 2. The torus shape approximation for coronal loops: *Top*: simple circular model with its linear representation. *Bottom*: footpoint vortex motion consequences: loops are approximately transformed respectively to a helix shape on a cylinder and into a line on a torus surface.

2.2. TARGET

The rapid emergence of a new active region (NOAA 8069) on August 5, 1997 made possible a study of the growth of its coronal loop system. This area – emerging shortly after the 1996 solar minimum cycle (Harvey and Hudson, 1998) – was far enough away from other active regions (Figure 1) to provide a good example of emerging flux tubes with rapid expansion and without interaction with other active regions (cf., also the MPEG movie in the CD-ROM).

3. Method to Compute the Size and Twist

3.1. THE GEOMETRY OF THE LOOP FITTING MODEL

A plasma loop traces the magnetic field from a positive polarity to a negative polarity. The simplest coronal loops can be described by the magnetic lines of a potential field configuration which corresponds to a minimum of the magnetic energy for a given vertical field at the photosphere (e.g., Aly, 1991). In many cases (Aschwanden *et al.*, 1999), loops can be fitted approximately with a circular model (i.e., constant radius without torsion in an Eulerian frame). A geometrical approxi-

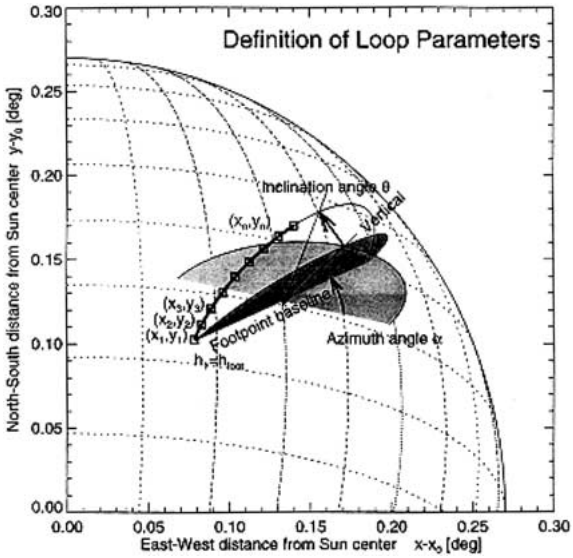

Figure 3. Geometric circular parameters definition with the standard circular approximation.

mation often used to describe a coronal loop is to neglect the global curvature of the loop, so the configuration is stretched and contained in a line between two 'half' planes representing the photosphere (Figure 2 top). We call F the transformation which, if applied to a circular loop, transforms it into a straight line.

In simple cases, footpoint motion will introduce torsion. In cylindrical coordinates, field lines are then transformed to a helix. By applying the reverse application F^{-1}, in 3D the field lines will approximately appear as lines upon a torus surface (Figure 2 bottom). It is worth noting that the force balance will be changed by this transformation. We neglect these effects here.

These non-circular and non-coplanar models are needed to describe twisted loops. More complex loop shapes, present even in bipolar magnetic regions are not considered in this paper.

3.2. ALGORITHM

As a first step, we consider that the loop is circular. We then determine the 3D parameters from *static stereoscopy*. In static stereoscopy, the solar rotation is used to vary the aspect angle of otherwise static structures (e.g., Loughhead, Chen, and Wang, 1984; Berton and Sakurai, 1985; Aschwanden and Bastian, 1994a, b; Davila, 1994; Aschwanden, 1995).

Recently, Aschwanden *et al.* (1999) have developed a method called *dynamic stereo vision* where the fit can be obtained even if the circular loops traces are not completely visible all the time (for the case where the closed magnetic field lines are not permanently traced). In this paper we want to take into account that the loop could be non circular. To be able to keep that possibility, our software uses

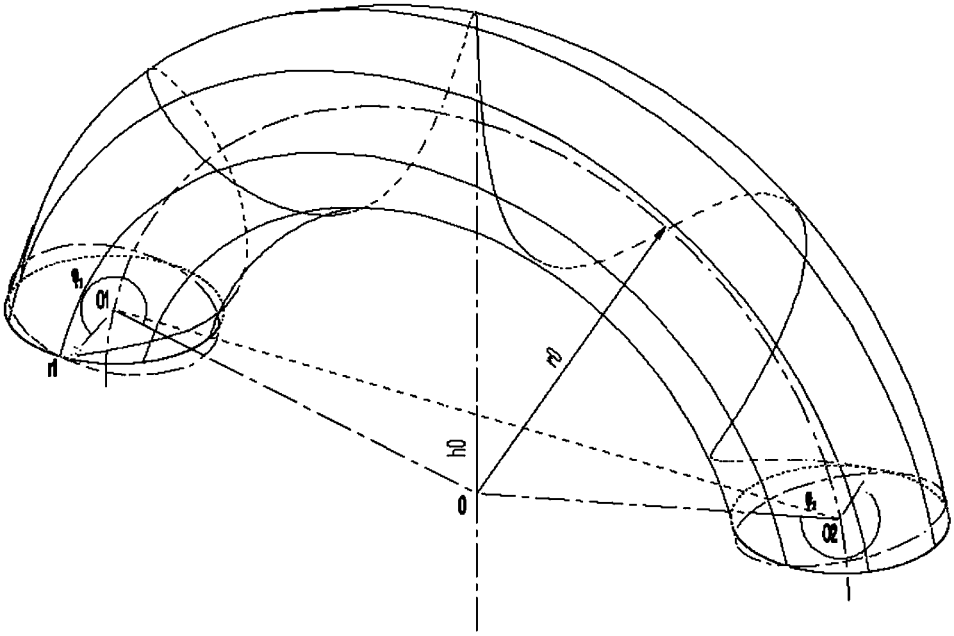

Figure 4. Definition of the parameters used to define a helix wound on a torus.

almost the same formula derived in steps 1 to 4 of paragraph 2.2 in Aschwanden *et al.* (1999, pp. 845–846). Each fitting is divided into 2 parts:

(1) A forward-fitting method of a given geometric model. The work is done on a single image where a geometric form is defined *a priori* and a best fit to one projection is done.

(2) Using pairs of images separated in time and assuming continuous change of parameters with time, we calculate the 3D geometry for twisted loops.

Afterwards if the circular fit shows a significant deviation from the observed loop we assume that the loop is on the torus to check if this deviation could be interpreted as a magnetic twist (as justified above).

The first model of coronal loop fitting (Figure 3) describes in a simplified way the morphology of the loops as circular arcs where radius r_0, altitude of the center over the photosphere h_0, azimuth and inclination angle (Az and ϑ) are determined. Different fitting parameters are found with an improved least square method (Powell function of IDL). Heliographic transformations used are presented in the Appendix A of Aschwanden *et al.* (1999).

When the loop is non circular, we replace the circular fitting (e.g., radius found R) by a *torus fitting* with the initial main radius $r_0 = R$, the small radius r_1 starts from zero and is fitted as the twist. This final fitting gives then, with time evolution: the torus radius r_0, its section radius r_1, the altitude above the photosphere h_0 and the position centers of the 2 cuts of the torus with the solar surface (S1 and S2). The program then gives how the line (loop) is twisted along the torus with Φ_1 and

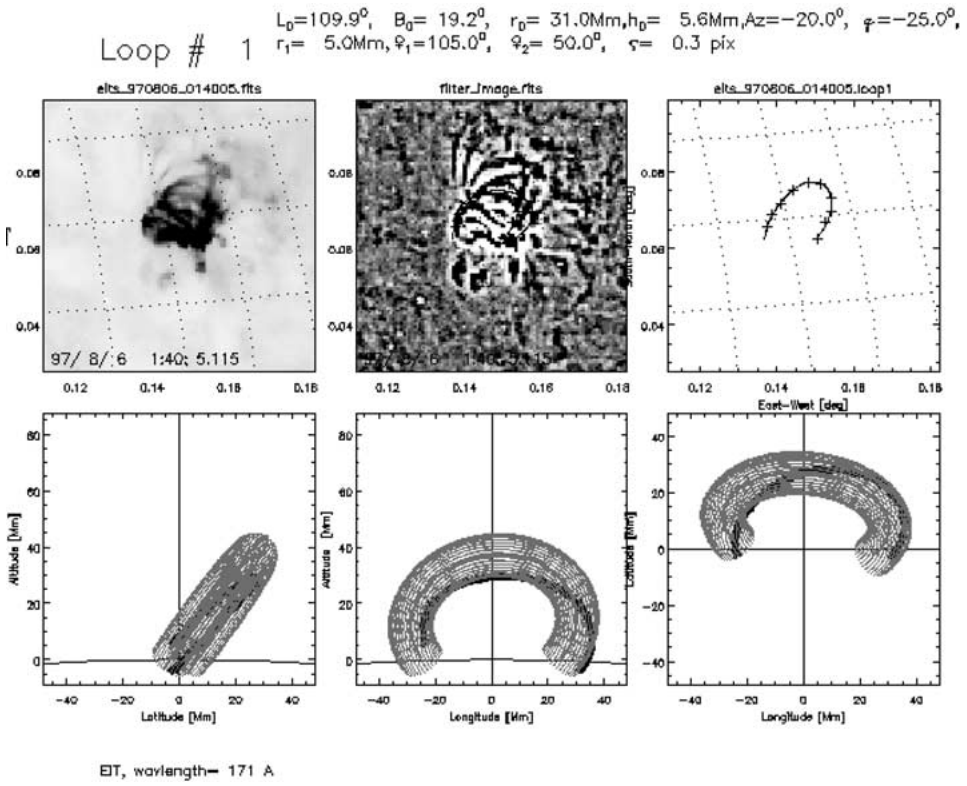

Figure 5. Example of the fit of one loop for 6 August 1997 at 01:40 UT. *On the upper left*: the EIT image and its transform with a Sobel filter which emphases the high spatial frequencies on the image. *On the upper right*: the determination of the loop on the image. *Lower images*: 3 different view points of the loop fit.

Φ_2 phase angles over sections S1 and S2. The complete twist Ψ is given by the difference between the two angles at the footpoints (Figure 4). The definitions of the origin of Φ_1 and Φ_2 are carefully chosen in such a way that if there is no twist Ψ is zero. It is important to note that each loop asymmetry is fully described by r_1, Φ_1, and Φ_2 or in an equivalent way by r_1, Φ_1, and Ψ (see Figure 4).

The fit is non linear, so in general there are several sets of parameters which minimize the distance between the observation and the model. Let us call s_i^j the jth solution for the fitted parameters ($(L_0)_i^j$, $(B_0)_i^j$, Az_i^j, ϑ_i^j, $(r_0)_i^j$, $(h_0)_i^j$, $(r_1)_i^j$, $(\Phi_1)_i^j$, $(\Phi_2)_i^j$) for the image number i.

From the different set of solutions we use the continuity obtained by stereo vision to derive the unique solution. For that, we select from the set of solutions s_i^j, the one with most continuous evolution of parameters. In practice, we first consider that the loops are circular. The heliographic latitude and longitude can be estimated by putting a spherical grid on the Sun. From two different images, it is easy to derive an initial estimation of the azimuth and inclination angles. These are the two

parameters that we derive first because the line of sight gives us a strong constraint. The sizes are then deduced. These provide starting values for the circular fit. If the deviation from the circular fit is too large we evaluate the twist as a perturbation of the circular model.

3.3. APPLICATION OF THE METHOD

As an example, the method is applied to the SOHO/EIT Fe IX/X image of 6 August 1997 at 01:40 UT (Figure 5). Loops (Figure 5(a)) are emphasized by Sobel filtering techniques (Figure 5(b)) as a high pass band filter. Loops are fitted with the described method. The tracing of a loop is established interactively on the image. It is plotted with crosses on Figure 5(c) while the result of the fitting obtained is drawn with a full line. Three different viewpoints are presented in Figures 5(d–f) to show the 3D geometry. The parameters deduced from the fitting are given at the top of Figure 5.

3.4. UNCERTAINTIES

To determine the exact coordinates and then the real morphology of the loops, we need to know with high accuracy the Sun center on the EIT images. The coordinates of the Sun center given by the FITS header is provided by an automatic fitting routine in which asymmetries, such as an active region on the limb introduce errors. Instead, we determine the Sun center by fitting a solar limb by a circle with 30 positions. It gives an accuracy of $\sigma = 1$ pixel$/30^{0.5} = 0.2$ pixel (EIT pixel size is about 2.616 arc sec). A more complete discussion can be found in Aschwanden *et al.* (1999).

We now discuss the error estimation of the values derived. As the precision on the image is 1 pixel and we fit loops with more than 10 points, the standard error introduced by describing the loop by a series of points is $\sigma = 1$ pixel$/10^{0.5} \approx 0.3$. Errors concerning the determination of latitude, longitude of loop position, azimuth angle and inclination angle are already discussed in Aschwanden *et al.* (1999). To derive the error for every other parameter, we measured successive images of each loop and analyzed the variation in each variable (while the other parameters were kept fixed). As EIT resolution is 2.6 arc sec, we obtained uncertainties of 2 Mm in linear dimensions. The loops studied have a size around 36 Mm, thus we are able to distinguish loops with 5 deg of twist differences (within the torus hypothesis). See the Appendix for details concerning measurement uncertainties.

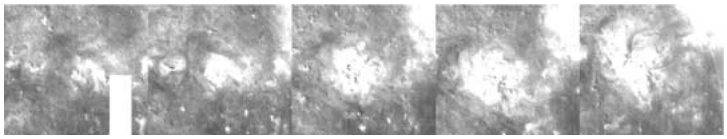

Figure 6. Intensity ratios 195Å/171Å, i.e., temperature between 0.7–1.5 MK (respectively *dark* – *bright*): 5 August 1997 at 07:00 UT, 13:00 UT, 19:00 UT, and 6 August 1997 at 01:00 UT, 15:00 UT.

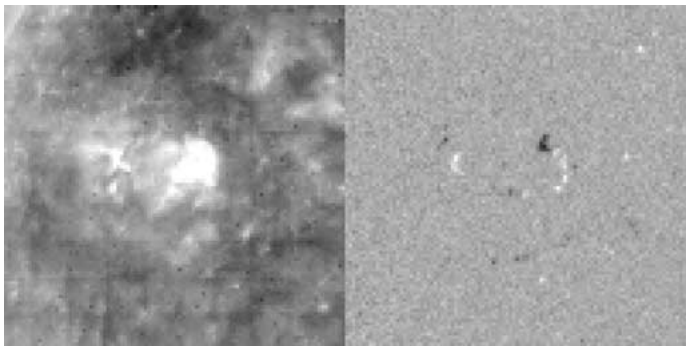

Figure 7. Aspect of the area with SOHO/EIT Fe IX/X et SOHO/MDI, 30 July 1997, i.e., 5 days before the appearance of the active region.

4. Observations of NOAA 8069

4.1. Before emergence

Active region NOAA 8069 emerged in an old activity location (Figure 7), as seen in some other cases (van Driel-Gesztelyi *et al.*, 1998). The remnant of the old active region (NOAA 8066) was weak. For example, on 30 July 1997, this coronal activity was seen by EIT as a diffuse area without distinguishable loops in agreement with MDI observations which showed a small bipolar magnetic field with weak intensity (Figure 7). The sunspot area in NOAA 8066 appeared at the limb on 25 July 1997 (*Solar Geophysical Data* Report, 1997) and was no longer visible on 31 July 1997 although it should have been near the disk center. The photospheric magnetic field remained weak but detectable (cf., iso-contours of the Stanford Magnetogram in *Solar Geophysical Data* Report, 1997). No structure was visible at the highest temperatures in X-rays with *Yohkoh*. No activity was reported until 5 August (*Solar Geophysical Data* Report, 1997) when the sunspot NOAA 8069 appeared there. New bright loops appeared on the EIT images on 5 August 1997 at 07:18 UT.

4.2. Active-region evolution

Loops were observed simultaneously in EUV-structures with temperatures around 10^6 K, and in X-rays $T_e \approx 5 \times 10^6$ K. The loops observed by EIT in NOAA 8069 do not appear to be simple potential loops corresponding to the bipolar photospheric

Figure 8. SOHO/MDI magnetic evolution of the bipolar AR: 5 August 1997 at 14:29 UT, 5 August 1997 at 15:27 UT, 6 August 1997 at 09:41 UT, 6 August 1997 at 17:28 UT. Magnetic field: *white* = positive polarity, *black* = negative polarity.

TABLE I

Loop size and twist evolution. Average of 5 different loops (the results for the different loops exhibit the same variations). We obtained uncertainties of 2 Mm for the maximum altitude and 5 deg for the twist. The small radius of the torus remains about 5 Mm.

Date time	5 Aug. 1997 19:07 UT	6 Aug. 1997 01:40 UT	6 Aug. 1997 15:51 UT	6 Aug. 1997 23:25 UT
Maximum altitude ($r_0 + h_0$ in Mm)	34	37	40	46
Twist: $\Psi = \Phi_2 - \Phi_1$	210	55	27	10
E.g., Loop 1a : Φ_2	230	105	70.1	50.3
E.g., Loop 1a : Φ_1	18	50	43	40

field observed (Figure 8). The fitting technique developed in Section 3 was used to estimate the twist in these loops.

From EIT images, first an increase of temperature was observed (Figures 6(a–c)). The increase of the temperature coincides with the position of the magnetic field lines which emerge. During the same time, magnetograms showed an enlargement of the bipolarity and an increase in the magnetic field intensity. This revealed strong development of photospheric magnetic activity (Figure 8) which is followed by an increase of temperature observed in the neighborhood of the loops and not only along the magnetic field lines (Figures 6(d) and 6(e)).

Five similar loops were fitted on each image. Then, the 3D loop geometry was obtained for 5 August 1997 at 19:07 UT (Figure 9(a)), the 6th at 01:40 UT (Figure 5), 6 August at 15:51 UT (Figure 9(b)), 6 August at 23:25 UT (Figure 9(c)).

Within the uncertainties, latitude, longitude and inclination angles were found to be the same for each loop which is consistent with the expected continuity in the evolution of loop parameters. Measured loop sizes and twists are summarized in Table I. The average loop expansion increased in height which is consistent with the development of the polarities observed at the photosphere (Figure 8). The loop size (altitude + main radius) increases with time.

The velocity of the average loop expansion is found to be less than a few km s^{-1}. After 2 days of quick expansion, the AR stabilizes in size.

The results of the fit (see Figure 5) give a left-handed helix (cf., definitions in Berger, 1998). This corresponds to a negative twist (T_w) and a negative helicity as the magnetic helicity is proportional to $T_w \Phi^2$ (Berger, 1985). As the region studied is in the northern hemisphere, this chirality agrees with the usual rules by hemisphere: for the northern hemisphere, the magnetic helicity is negative (Seehafer, 1990; Pevtsov, Canfield, and Metcalf, 1995).

The main result is that the measured twist (Table I) decreased continuously with time during the increase of loop size. The coherent evolution found for the fitting parameters gives some confidence in the technique developed in Section 3. The main result is that the measured twist is decreasing with time during the emergence of AR 8069. The difference of sign between T_w and ψ comes from the geometrical definition. The evolution is analyzed in the next section.

5. Analysis

5.1. Active-region emergence

We have analyzed the formation of a new active region where a set of loops was visible in UV. Our observations show that these loops were twisted when they first appeared in the corona (Table I). In the same way as Leka *et al.* (1996), we interpret our observations as the emergence of a twisted flux tube. However, one difference is that Leka *et al.* observed the emergence of 5 small bipoles in an already existing active region, while in our case it is the full active region which is emerging.

Such emergence of a twisted flux tube is expected from the recent development of the theory analyzing the transport of magnetic flux from the bottom of the convection zone to the photosphere. Indeed both Emonet and Moreno-Insertis (1998) and Fan, Zweibel, and Lantz (1998) show independently that a minimum of magnetic twist is needed in order that the flux tube keeps its coherence during its rise through the convective zone.

5.2. Evolution in the corona

What is the expected evolution in the corona of such a flux tube? As the emergence proceeds, a larger part of the twisted flux tube is present in the corona, thus, without dissipation, the twist is expected to grow up to a maximum value (when the remaining part of the flux tube in the convective zone is no longer buoyant). This increase of coronal twist has probably happened in our analyzed case earlier in time but it was difficult to visualize the loop in EUV in this early stage of the emergence (before 19:00 UT on 5 August). Rather, when we were able to follow the loops, a continuous decrease of twist was observed (Table I). Since the magnetic twist is closely related to the non-potentiality of the magnetic field and thus to its free energy, the decrease of twist may be interpreted as the consequence of magnetic dissipation. In particular it is well known that a potential magnetic field, with no

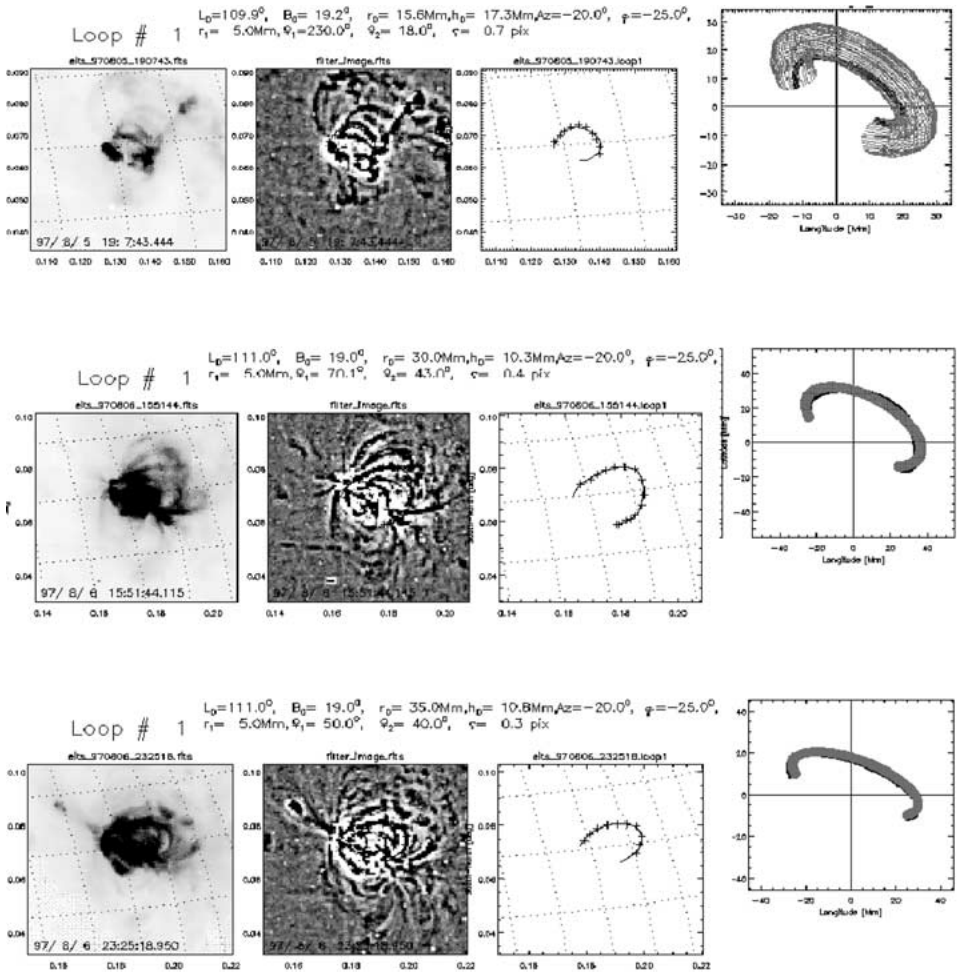

Figure 9. Loops fitting: radius, altitude and twist measured for the 3 other images. *From left to right*: the EIT image studied, its Sobel transformed with the loop pointing overlaying, the pointing and the result of the fitting. *From up to down*: the results are given for 5 August 1997 at 19:07 UT, the 6 August at 15:51 UT, and 23:25 UT.

twist, minimizes the magnetic energy for a given distribution of the vertical component of the photospheric magnetic field. Before further analyzing this scenario, we describe the constraints given by the observations on the dissipation mechanism.

How was the energy dissipated? In the case of NOAA 8069 flares were detected only after 6 August (as shown by EIT and GOES data). So the excess of energy was not realized in flares or it could be that the event intensities were less than the instrument sensitivity.

No CME either was detected in association with this active region (LASCO Team, 1999). The only evidence of dissipation is the presence of hot loops in the active region (Figure 6) which expand. This corresponds to a global heating of the

loops and may explain the decrease of magnetic twist (while the energy budget of the emission is difficult to estimate from observations with the narrow pass-band filters of EIT).

5.3. Relaxation of the magnetic field

According to the above section, the dissipation of the magnetic energy, associated with the twist, appears to be the most plausible interpretation of the twist evolution. However, this needs further analysis because a constraint arises from the conservation of magnetic helicity H in resistive MHD. It is dissipated much more slowly than the magnetic energy in magnetized plasma with a high Lundquist number such as the coronal medium, (Biskamp, 1993). For a closed magnetic volume (i.e., without flux exiting from the surface of the volume), magnetic helicity is simply defined by the integral over the volume $\mathbf{H} = \int\int\int \mathbf{A} \cdot \mathbf{B}\, \mathrm{d}^3\mathbf{r}$, where $\mathbf{A}$ is the vector potential of $\mathbf{B}$.

For an open system, like the magnetic field of an AR above the photosphere, this definition needs a generalization : the definition of a relative helicity. But the important point here is that this relative helicity is also preserved provided there is no injection of helicity through the boundary – here the photosphere (Berger and Fields, 1984). The conservation of helicity implies that the lowest energy level (the potential field) cannot be reached if the field is contained in a finite volume. The field with minimum energy, with the same photospheric distribution of the vertical field component, is instead a non-linear force-free field (Sakurai, 1981). The relaxation to this field still allows a decrease of the magnetic twist. However in the corona the plasma beta is low so that the magnetic field is space-filling. The newly emerged field will expand until there is a force balance with the ambient coronal field. In general this will produce current sheets where magnetic energy will be dissipated, and where part of the helicity will be transfered to the ambient field.

We finally conclude that the magnetic twist of the emerging flux tube could plausibly decrease to a low value, both because of the large expansion of the flux tube in the corona and because part of the magnetic helicity is transferred to the surrounding corona (so cascading to large spatial scales, see, e.g., Biskamp, 1993). This proposition needs however to be tested quantitatively with MHD numerical simulations.

6. Conclusion

With the development of a new fitting technique based upon stereoscopy of EIT images we are able to find 3D parameters for loops such as their size and twist. The emergence and the evolution of active region loops without magnetic neighborhood interaction is tracked.

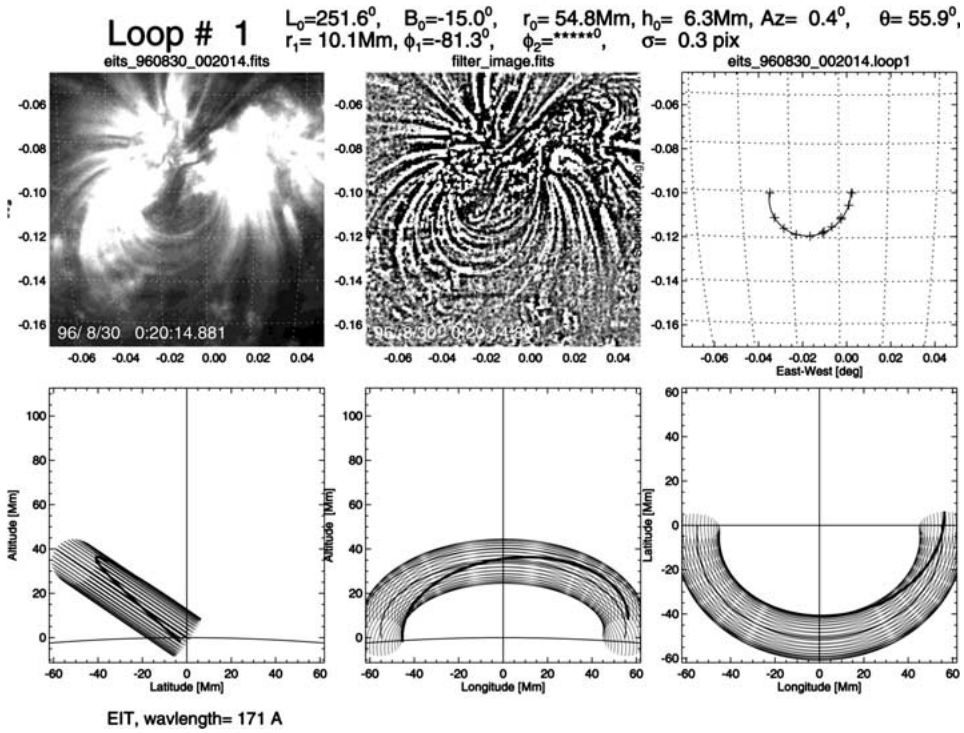

Figure 10. SOHO/EIT 30 August 1996 at 00:20:14 UT, loop 1. Parameter fitting gives $l_0 = 251.62$, $b_0 = -15.02$, $r_0 = 54.84$ Mm, $h_0 = 6.28$ Mm, az $= 0.45$, th $= 55.86$, $r_1 = 10.05$ Mm, $\phi_1 = -81.33$ deg, $\phi_2 = -197.10$ deg. Measured error between the model and the fit is 0.32 pixel.

Active region loops in NOAA 8069 were twisted (almost one turn) when first observed and de-twisted with time as the loops expanded. The de-twisting with expansion can be explained by considering the conservation of helicity while the twist is transfered into an adjacent volume of the corona.

We can try to speculate about what happens if the anisotropy of the emerging flux is too large to be relaxed in a decent time scale. Thus the expansion could happen very quickly and create a plasmoid ejection. Amari *et al.* (1996a,b) have already discussed the impact of the shear to CMEs. Some flares are related with twisted or shared emerging flux (Ambastha, 1997; Ishii and Kurokawa, 1997). Measurement of twist between flare and emergence needs to be done in the future to confirm this possible scenario. This method could better constrain loop flare prediction for space weather forecasting.

Additional Material on the CD-ROM

The MPEG arem97 movie was made from the EIT full-disk full-resolution (1024×1024 pixels) images available in the transition region Fe IX/X line (171Å). Images

were taken 5 August at 01:05, 07:18, 13:23, 19:18, and 6 August at 01:40, 07:53, 15:39, 17:35, 19:00, 19:54, 22:46 UT. The movie displays the emergence and growth of the ARLs of NOAA 8069.

Acknowledgements

F. Portier-Fozzani thanks for support during the PhD thesis – which partially led to this work – Francis Rouard, the Rotary-Club of Roquefort Les Pins (president Pierre Baude) and the philosophical circle: 'Edgar Morin, la Pensée Complexe' (president Bernard Kohl). He also thanks Serge List for graphics, Roger Malina and Andre Jean Maucherat for advice in writing the paper. Part of the work has been done while the main author was at the Laboratoire d'Astronomie Spatiale in Marseilles (CNRS UPR, France) with the support of the laboratory and the EIT Team. The authors also wish to thank an anonymous referee for comments which helped to improve the paper.

Appendix : Method Validation and Uncertainty Measurement

A complete analysis concerning validation of the method and the uncertainty measurement has been done using August 1996 data (Portier-Fozzani, 1999). The file eits_960802_072407.loop1 for 2 August 1996 at 07:24 UT includes loop 1 coordinates as on a screen showing the SOHO/EIT image. These coordinates will be transformed with the ephemerides and the heliographic position for the different fitting.

Several examples of parameter fitting are given in Table II (file eits_960802_072407.para1).

Some of these values, which are not physical (such as an inclination angle more than 90 deg which would correspond to a structure under the solar surface), are suppressed. Meanwhile, we obtain several values for the fitting with only one image. The uniqueness of the solution is obtained in comparing data from images given in a time sequence. Values obtained with different images must be close while the magnetic flux is continuously moving (in the mathematical sense). It is then possible to re-plot the corrected fitted loop.

A.1. Uncertainties

We check the uncertainties (Figures 10 and 11) for all the processed parameters.

As an example on the data of 30 August 1996, if instead of $\phi_2 = -197.10$ deg we would have $\phi_2 = -190$ deg, then the difference between the model and the fitting plot will grow 0.32 pixel up to 2.78 pixels. So the minimization of these differences is effective down to 7 degrees of twist difference.

TABLE II

Several geometrical solutions obtained for one loop with one angle only (variation between the model and the fit -dev- is given in pixels).

l_0	b_0	r_0	h_0	az	th	r_1	$\Phi 1$	$\Phi 2$	dev
254.24	−7.95	57.16	9.77	18.91	−92.56	2.92	301.73	138.35	1.15
256.29	−7.58	58.11	1.39	32.67	−86.87	25.01	145.79	−39.05	1.73
254.26	−8.02	54.65	10.11	28.99	−74.45	1	0.0	1	0.73
254.52	−7.79	64.93	16.49	16.09	−97.01	19.21	228.96	118.75	1.22
254.62	−9.27	52.61	24.22	14.21	−94.59	0.12	39.00	55.27	1.13
254.51	−6.35	62.26	13.31	15.56	−57.93	18.71	122.27	104.08	2.85
254.52	−6.34	62.28	13.48	15.47	−58.02	18.91	122.60	103.49	2.84

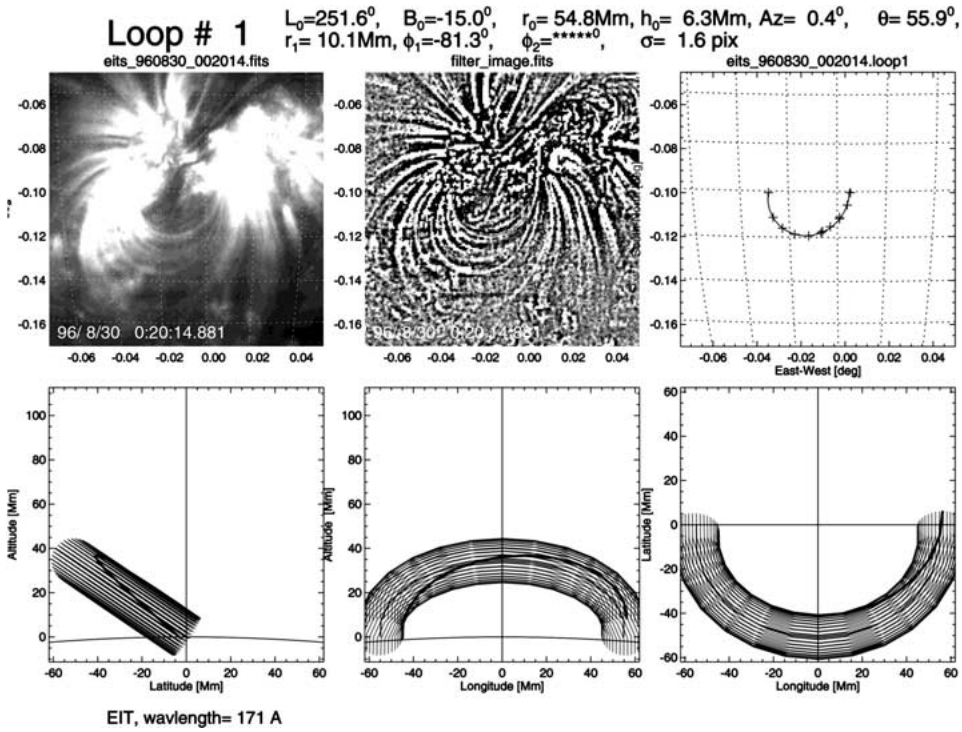

Figure 11. SOHO/EIT 30 August 1996 at 00:20:14 UT, loop 1. Parameters fitted are chosen such as $l_0 = 251.62$, $b_0 = -15.02$, $r_0 = 54.84$, $h_0 = 6.28$, $az = 0.45$, $th = 55.86$, $r_1 = 10.05$, $\Phi_1 = -81.33$, $\Phi_2 = -190$, giving a measured error between the model and the fit of 2.78 pixels.

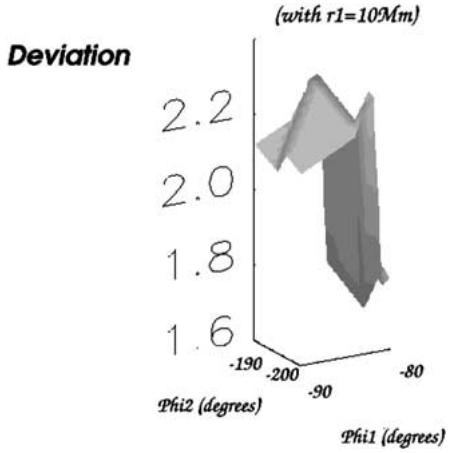

Figure 12. For r_1 given at 10 Mm, minimal variation obtained for ϕ_1 from -90 to -80 deg, ϕ_2 from -200 to -190 deg: minimum deviation correspond to $\phi_1 \sim -81$ deg and $\phi_2 \sim -197$ deg.

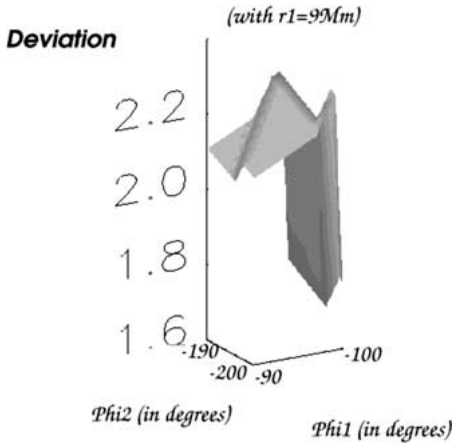

Figure 13. For r_1 given at 9 Mm, measurement of the minimum variation for ϕ_1 from -90 up to -80 deg, ϕ_2 from -200 up to -190 deg.

The uncertainty calculation is given by the sum of all uncertainties for each of the parameters. With 30 points, a previous calculation (in the main text) shows that the most discernible difference between the sampled loop and the model is an error of 0.2 pixels. If s_1 is the solution and s_2 can be a solution if $\text{Error}(\text{Norm}(s_2 - s_1)) \leq 0.2$ pixels. Then for all fixed parameters except Φ_2, this cooresponds numerically to $\Delta\Phi \sim 4.7$ deg (Portier–Fozzani, 1999). Numerical simulations for the uncertainties is used because even if the torus is a correct analytical function, a line over a torus is not a simple function and the error cannot be easily derived.

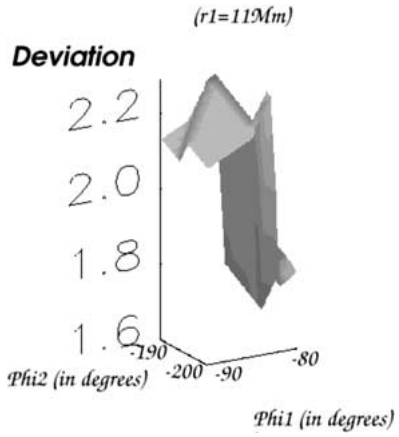

Figure 14. For r_1 fixed at 11 Mm, measurement of the minimum variation for ϕ_1 from -90 to -80 deg, ϕ_2 from -200 to -190 deg.

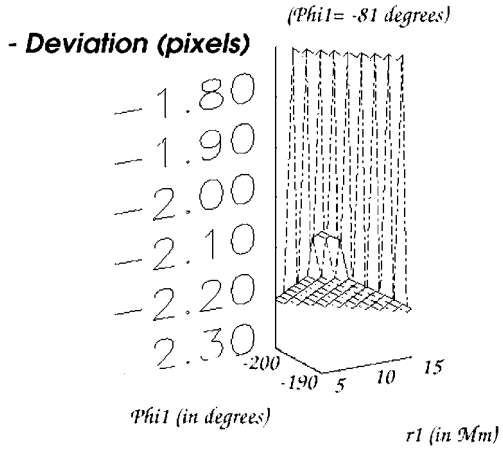

Figure 15. For ϕ_1 fixed at -81 deg, deviation as a function of r_1 and ϕ_2: The minimum is reached for $r1 \sim 10$ Mm and $\phi_2 \sim -197$ deg.

A.2. Global Minimization convergence

Table III gives the solution found for 30 August 1996 at 0 h 20 min 14 s.

TABLE III
Converged values found by the method.

l_0	b_0	r_0	h_0	az	th	r_1	$\Phi1$	$\Phi2$	dev
251.62	−15.02	54.84	6.28	0.45	55.86	10.05	−81.33	−197.10	0.32

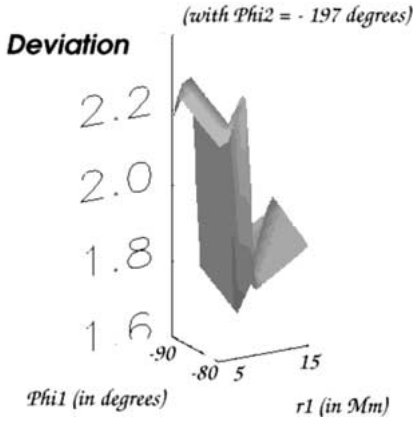

Figure 16. For ϕ_2 fixed at -197 deg, deviation as a function of r_1 and ϕ_1: the minimum is reached for $r_1 \sim 10$ Mm and $\phi_1 \sim -81$ deg.

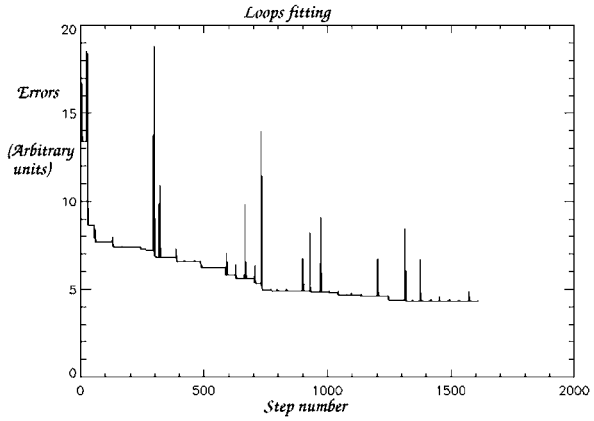

Figure 17. Minimization of dev as a function of the step number.

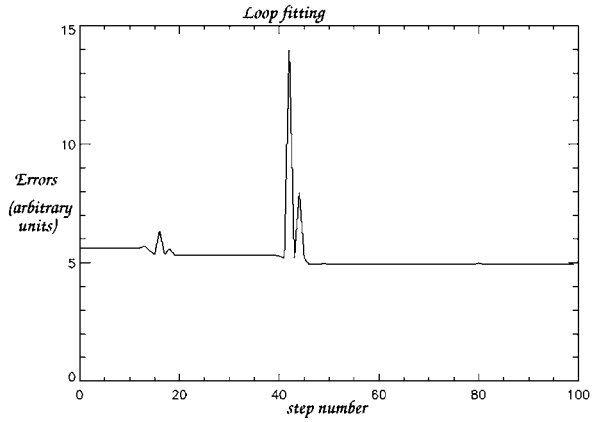

Figure 18. Minimization of dev with entropy minimum method (deviation as function of the step).

We show that this solution completely minimizes the error over all sets of parameters by analyzing how the method works.

Let us take the initial value as $l_0 = 262$ deg, $b_0 = -15$ deg, $r_0 = 55$ Mm, $h_0 = 6$ Mm, $az = 0$, $th = 56$, while r_1 goes from 5 to 15 Mm with 1 Mm step, ϕ_1 from -90 to -80 deg with $+1$ deg step, ϕ_2 from -200 to -190 degrees with $+1$ deg step. Then we can analyze the deviation versus (ϕ_1,ϕ_2) for $r_1 = 10$ Mm. In practice, we would try 2 other values of r_1 to look at the variations of the other parameters.

The minimum is reached (Figure 12) for $\Phi_1 = -81$ deg and $\Phi_2 = -197$ deg. While comparing Figures 12–14, this minimum is a minimum over a certain topological neighborhood. To check that, we have to consider also variations with r_1 (Figures 15 and 16), and thus a global formula is derived from the variational calculation over the set of all variables.

A.3. Convergence

The method is converged by minimizing the error parameter dev. Several steps for the method are shown in Figures 17 and 18.

Because the Powell function uses a kind of entropy minimalization, the program is able to jump over a local gap from a local minimum to the global minimum. Then the program converges toward the absolute minimum of the deviation over the set of all variables.

A.4. Conclusion for the method

The method, based on Powell procedures, reaches a global minimum of the difference between a graphical fit and a model. Complete uncertainty formulas can not be calculated directly by analytical mathematics but errors can be estimated by looking at the difference introduced by a small change in the parameters. Reasonable values obtained (e.g., with a big difference change while the angle does not change more than 5 degrees) confirm the good accuracy of the method.

References

Aly, J. J.: 1991, in B. Schmieder and E. Priest (eds.), *Dynamics of Solar Flares*, Flares 22 Workshop, Obs. Paris-Meudon, p. 29.

Amari, T., Luciani, J. F. *et al.*: 1996a, *Astron. Astrophys.* **306**, 913.

Amari, T., Luciani, J. F., Aly, J. J. *et al.*: 1996b, *Astrophys. J.* **466**, L39.

Ambastha, A.: 1997, in K. S. Balasubramaniam, J. Harvey, and D. Rabin (eds.), *18th NSO/Sacramento Peak Summer Workshop Synoptic Solar Physics*.

Aschwanden, M. J.: 1995, *Lecture Notes Physics* **444**, 13.

Aschwanden, M. J. and Bastian, T. S.: 1994a, *Astrophys. J.* **426**, 425.

Aschwanden, M. J. and Bastian, T. S.: 1994b, *Astrophys. J.* **426**, 434.

Aschwanden, M. J., Newmark J. S., Delaboudinière, J. P. *et al.*: 1999, *Astrophys. J.* **515**, 842.

Bentley, R., Mariska, J. T., and Sakao, T.: 1996, *Publ. Astron. Soc. Pacific* **109**, 107.
Berger, M.: 1985, *Astrophys. J. Suppl. Ser.* **59**, 433.
Berger, M. and Fields, 1984, *Geophys. Astrophys. Fluid Dyn.*, **30**, 79.
Berton, R. and Sakurai, T.: 1985, *Solar Phys.* **96**, 93.
Biskamp, D., 1993, *Nonlinear MHD*, Cambridge Monographs on Plasma Physics.
Bray, R. J., Cram, L. E., Durrant, C. J., Loughhead R. E.: 1991, *Plasma Loops in the Solar Corona*, Cambridge Astrophysics Series.
Davila, J. M.: 1994, *Astrophys. J.* **423**, 87.
Delaboudinière, J. P. *et al.*: 1995, *Solar Phys.* **162**, 291.
Dere, K. P., Brueckner, G. E., Howard R. A. *et al.*: 1997, *Solar Phys.* **175**, 601.
Emonet, T. and Moreno-Insertis, F.: 1998, *Astrophys. J.* **492**, 804.
Fan, Y., Zweibel E. G., and Lantz, S. R.: 1998, *Astrophys. J.* **493**, 480.
Harvey, K. L. and Hudson, H. S.: 1998, in *Observational Plasma Astrophysics: Five Years of Yohkoh and Beyond*, Astrophysics and Space Science Library, Dordrecht Kluwer Academic Publishers, pp. 229, 315.
Heyvaerts, J. and Hagyard, M.: 1991, in B. Schmieder and E. Priest (eds.), *Dynamics of Solar Flares*, Flares 22 Workshop, Obs. Paris-Meudon, p. 1.
Ishii, T. T. and Kurokawa, H.: 1997, *Physics of the Sun and Heliosphere in the Era of Space Probes: Scientific Highlights of SOHO, Ulysses, and Yohkoh*, 23rd IAU Meeting.
Klimchuk, J. and Porter, L.: 1996, 'Magnetodynamic Phenomena in the Solar Atmosphere', *IAU Colloquium* **153**, 39.
LASCO Team, 1999, http://lasco-www.nrl.navy.mil/cmelist.html.
Leka, K. D., Canfield, R. C., McClymont, A. N., and van Driel-Gesztelyi, L.: 1996, *Astrophys. J.* **462**, 547.
Loughhead, R. E., Chen, C. L., and Wang, J. L.: 1984, *Solar Phys.* **92**, 53.
Newmark, J., 1997, *Temperature and density with SOHO/EIT*, EIT internal report.
Neupert, W., Delaboudinière, J. P., Thompson, B. *et al.*: 1998, *Solar Phys.* **183**, 305.
Parker, E. N.: 1974, *Solar Phys.* **36**, 249.
Pevtsov, A. A., Canfield, R. C., and Metcalf, T. R.: 1995, *Astrophys. J.* **440**, L109.
Portier-Fozzani, F.: 1999, Ph.D. Thesis (in French), *The 3D Solar Corona and its Evolution with SOHO/EIT*, University of Nice Sophia Antipolis and Laboratoire d'Astronomie Spatiale (France), (available on CD-ROM and online http://www.linmpi.mpg.de/ fabrice/)
Portier-Fozzani, F. *et al.*: 1997, *Publ. Astron. Soc. Pacific Conf. Ser., IAU Colloq.* **167**.
Rust, D. and Kumar, A.: 1996, *Astrophys. J.* **464**, L199.
Sakurai, T.: 1981, *Solar Phys.* **69**, 343.
Seehafer, N.: 1990, *Solar Phys.* **125**, 219.
Solanki, S.: 1998, *Lecture Notes in Physics*, **507**, 41.
Solar Geophysical Data Report, *NOAA*, 1997.
Uchida, Y.: 1992, *Publ. Astron. Soc. Japan* **44**, L181.
Van Driel-Gesztelyi, L. *et al.*: 1998, *Publ. Astron. Soc. Pacific Conf. Ser.* **155**, 202.